9294–9305 *Nucleic Acids Research, 2022, Vol. 50, No. 16* *Published online 29 July 2022*
https://doi.org/10.1093/nar/gkac651

Stochastically multimerized ParB orchestrates DNA assembly as unveiled by single-molecule analysis

Lijuan Guo[1,†], Yilin Zhao[1,†], Qian Zhang[1,2,3,6], Ying Feng[1,4], Lulu Bi[1], Xia Zhang[1], Teng Wang[1], Cong Liu[5], Hanhui Ma[1] and Bo Sun[1,*]

[1]School of Life Science and Technology, ShanghaiTech University, Shanghai 201210, China, [2]CAS Center for Excellence in Molecular Cell Science, Shanghai Institute of Biochemistry and Cell Biology, Chinese Academy of Sciences, Shanghai 200031, China, [3]University of Chinese Academy of Sciences, Beijing 100049, China, [4]School of Biotechnology, East China University of Science and Technology, Shanghai 200237, China, [5]Interdisciplinary Research Center on Biology and Chemistry, Shanghai Institute of Organic Chemistry, Chinese Academy of Sciences, Shanghai 201210, China and [6]Present address: School of Chemistry and Chemical Engineering, Frontiers Science Center for Transformative Molecules and National Center for Translational Medicine, Shanghai Jiao Tong University, Shanghai 200240, China

Received April 12, 2022; Revised July 11, 2022; Editorial Decision July 11, 2022; Accepted July 19, 2022

ABSTRACT

The tripartite ParAB*S* system mediates chromosome segregation in a wide range of bacteria. Dimeric ParB was proposed to nucleate on *parS* sites and spread to neighboring DNA. However, how properly distributed ParB dimers further compact chromosomal DNA into a higher-order nucleoprotein complex for partitioning remains poorly understood. Here, using a single-molecule approach, we show that tens of *Bacillus subtilis* ParB (Spo0J) proteins can stochastically multimerize on and stably bind to nonspecific DNA. The introduction of CTP promotes the formation and diffusion of the multimeric ParB along DNA, offering an opportunity for ParB proteins to further forgather and cluster. Intriguingly, ParB multimers can recognize *parS* motifs and are more inclined to remain immobile on them. Importantly, the ParB multimer features distinct capabilities of not only bridging two independent DNA molecules but also mediating their transportation, both of which are enhanced by the presence of either CTP or *parS* in the DNA. These findings shed new light on ParB dynamics in self-multimerization and DNA organization and help to better comprehend the assembly of the ParB-DNA partition complex.

INTRODUCTION

During cell division, faithful chromosome segregation ensures the inheritance of a full copy of the genetic information of the parent to each daughter cell (1–4). In many bacterial species, chromosome segregation relies on the tripartite ParAB*S* system, consisting of an ATPase protein ParA, a DNA-binding protein ParB, and a centromere-like palindromic DNA sequence, named the *parS* site (5). In a typical ParAB*S* system, ParB proteins first recognize and specifically bind to clusters of the *parS* sites, followed by association with *parS*-flanking regions (6–8). DNA-bound ParB proteins condense the chromosomal DNA into a large higher-order nucleoprotein complex and facilitate the formation of a poorly organized network of DNA loops (6). This kinetochore-like structure, also known as the partition complex, serves as a functional assembly that can recruit the P-loop ATPase ParA (9). A gradient of nucleoid-associated ParA-ATP dimers created by the stimulation of the ATPase activity of ParA provides a driving force to move the partition complex, and hence the sister replicon(s), to the opposite side of the cell (10,11). In addition to chromosome segregation, ParB sometimes has additional species-specific functions. For example, in *B. Subtilis*, ParB (Spo0J) facilitates the recruitment of the structural maintenance of chromosome (SMC) complex and contributes to origin localization (12–14); In *Caulobacter*, ParB forms a complex with MipZ and together regulates cell division (15). Therefore, ParB plays multifaceted roles and the ParB-DNA complex is essential for the recognition, organization, replication, and partitioning of DNA molecules.

The assembly of the partition complex begins with ParB dimers nucleating on *parS* sites and later associating with neighboring DNA, a process termed 'spreading' (16). Recently, a series of studies have revealed a new factor in ParB spreading: CTP (17–23). ParB and ParB-like proteins are

*To whom correspondence should be addressed. Tel: +86 21 20684536; Fax: +86 21 20685430; Email: sunbo@shanghaitech.edu.cn
†The authors wish it to be known that, in their opinion, the first two authors should be regarded as Joint First Authors.

CTPases that can bind and hydrolyze CTP (17,18). In the presence of CTP, a ParB dimer forms a clamp-like structure and encircles double-stranded (ds) DNA in the center of the clamp (19,21,22). The CTP-bound ParB dimer at the *parS* site weakens its association with DNA, allowing them to dissociate from the site and diffuse to neighboring low-affinity DNA (19–21,24). In addition to the loading and spreading of ParB dimers on the chromosomal DNA, the formation of a higher-order ParB-DNA complex necessitates the coalescence of multiple ParB dimers into nanometer-sized condensates as evident by *in vivo* experiments, which drives DNA co-condensation (25,26). As the intracellular concentration of ParB is not high enough to grow an extensive filament on DNA (27–29), ParB-mediated DNA looping was proposed to explain the co-condensation of ParB and DNA (29). In this model, long-distance DNA up to 10–20 kb is looped via ParB–ParB and ParB–DNA interactions, thus condensing DNA into a loosely compacted structure. In support of this looping model, single-molecule experiments provided a few pieces of *in vitro* evidence to display the DNA bridging and condensation activities of ParB, which exhibited a dependence on both *parS* and CTP (20,29). Recently, a nucleation and caging model was proposed to better explain how *parS* sites act as a nucleation center, allowing ParB clusters to restrain the chromosomal DNA into a spatially confined space (26,30,31). However, despite extensive studies, our knowledge of how hundreds of ParB dimers centered around the *parS* sites effectively assemble to form condensates for the organization and compaction of chromosomal DNA is still limited.

Bacillus subtilis genetically encodes a ParB homologue named Spo0J, which mediates chromosome segregation during sporulation (32). *In vivo*, Spo0J proteins assemble into single foci that colocalize with the *oriC* region of the chromosome, and together with Soj (ParA homologue in *B. subtilis*), contribute to the timely separation of replicated origins (14,33). Notably, in addition to the specific binding to eight *parS* sites scattered around the *oriC* region, Spo0J in a dimeric form spreads and associates with several kilobases of nonspecific DNA flanking *parS* sites (34,35). Therefore, Spo0J serves as a model system for the understanding of the dynamic assembly of the ParB–DNA complex. In this study, by combining optical tweezers with confocal fluorescence microscopy, we examined the dynamic association and disassociation of Spo0J (hereafter referred to as ParB) on DNA at the single-molecule level. We found that tens of ParB proteins can stochastically multimerize on and off nonspecific DNA. In the presence of CTP, the ParB multimer actively diffuses along DNA with coefficients of 0.1–0.4 kb^2/s and yet preferentially remains immobile on *parS* sites. After a collision, two ParB multimers have a chance to fuse as one. Strikingly, the ParB multimer is distinguished from the ParB dimer in its unique capabilities to bridge two DNA molecules and shift their relative positions. These findings suggest that the ParB multimer not only organizes chromosomal DNA but also provides a means to condense the dimeric ParB into foci, possibly serving as a functional intermediate in partition complex assembly.

MATERIALS AND METHODS

Preparation of DNA templates

The λ phage DNA template was constructed as described elsewhere (36). Briefly, biotinylated λ DNA was constructed through 3′-end labeling by filling in 5′-overhangs with an exo-Klenow fragment. The reaction was conducted by incubating 10 nM λ DNA (Thermo Scientific), 250 μM dGTP/dATP/dTTP, 10 μM biotin-14-dCTP (Thermo Scientific), and 5 U Klenow exo⁻ (Thermo Scientific) in reaction buffer (50 mM NaCl, 10 mM Tris–HCl pH 7.9, 10 mM $MgCl_2$ and 1 mM DTT) at 37°C for 1 h, followed by heat inactivation for 10 min at 75°C. The mixture was purified by Column DNA Purification Kit.

The DNA template containing 1× or 8× *parS* sites was the ligation product of three DNA segments, L1, L2, and the *parS* segment (Supplementary Figure S1A). The 7.6-kb L1 and 12.9-kb L2 DNA segments were polymerase chain reaction (PCR)-amplified from λ DNA. The resulting DNA fragments were digested with BstXI (NEB) to create an overhang for ligation. The *parS* DNA segment containing the 1x *parS* site was obtained by annealing two oligonucleotides in annealing buffer (20 mM Tris–HCl pH 8.0, and 100 mM KCl) (Supplementary Table S1). The partial match of the two oligonucleotide sequences allows for the creation of two overhangs at each end for ligation. The 8x *parS* DNA segment was produced by PCR from the modified plasmid pDONOR4.1 (Supplementary Table S1). The PCR product was digested with BstXI to create overhangs for ligation. The final product was produced by ligating the L1, L2 and *parS* segments at a 1.2:1.2:1 ratio using T4 DNA ligase (NEB).

To construct the 18.6-kb *parS*-containing template, a 544-bp DNA segment containing 8x *parS* was amplified from the modified plasmid pDONOR4.1 (Supplementary Figure S1B). This segment was inserted into a 13.4-kb lenti-CRISPRi plasmid (Supplementary Table S1). The resulting DNA ligation product (13.8 kb) was digested and linearized with KpnI and NheI (NEB). Another 4.8-kb DNA segment containing 8× *parS* was PCR-amplified and inserted into the 13.8-kb vector using the ClonExpress II One Step Cloning Kit (Vazyme). The 18.6-kb *parS*-containing template termed L4 was PCR-amplified from the resulting 18.6-kb plasmid. The nonspecific 18.6-kb DNA template termed L5 was amplified by PCR using λ DNA as a template.

Protein expression and purification

ParB-eGFP. The C-terminally eGFP-fused ParB protein from *B. subtilis* (ParB-eGFP) was expressed and purified as follows. The *parB* gene was amplified and constructed in a pET-based expression vector, which consists of a sequence encoding eGFP and an C-terminal His_6-tag. The protein was expressed in *Escherichia coli* strain BL21 (DE3) (TransGen) cells. The cells were grown in Kanamycin resistance-contained LB medium at 37°C for 4 h. When the optical density at 600 nm reached 0.6, protein expression was performed at 18°C for 16 h following induction with 1 mM isopropyl-beta-D-thiogalactopyranoside. The medium was then discarded. The harvested cells were lysed in 1 mM

EDTA, 300 mM NaCl, 50 mM Tris–HCl pH 7.5 and 1% protease inhibitor and filtered through a 0.22-μm Millipore Express® PES Membrane Filter Unit. The cells were disrupted by passing through a high-pressure cell crusher at ∼800 bar three times. The lysed solution was then centrifuged at 11 000 rpm for 60 min, and the clarified supernatant from the cell lysate was separated from the cellular debris and bound in batch to Ni-NTA Agarose (TransGen). The column was further washed by lysis buffer containing different imidazole concentrations of 5, 20, 50 and 200 mM. The bulk of ParB-eGFP was in the 50 mM imidazole eluate. The eluate was then concentrated using 50-kDa filtration at 5000 rpm to a certain volume at 4°C. ParB-eGFP was further purified with gel filtration chromatography with a Superdex 200 increase 10/30 column (GE Healthcare) in storage buffer (50 mM Tris–HCl pH 7.5, 300 mM NaCl, and 10% (v/v) glycerol). Consistent with wild-type ParB (17) (37), the purified ParB-eGFP protein was verified to preferentially exist in a dimeric form and display both CTPase and DNA binding activities comparable to those of wild-type ParB (Supplementary Figure S2). The two ParB mutants (R80A and N112S) were expressed and purified similarly.

ParB-Cy5 and ParB-AF555. Since ParB contains no native cysteine residues, the vector was designed to contain a cysteine before the N-terminal tag that was used to covalently coupled with a maleimide-conjugated fluorophore (Cy5 or AF555). Fluorophore labeling was conducted in 50 mM Tris–HCl pH 7.5, 300 mM NaCl, 10% (v/v) glycerol and a 10-fold molar excess of Cy5-maleimide dye or AF555-maleimide at 4°C for 12 h. To remove free fluorophores, the conjugate solution was centrifuged at 5000 rpm in storage buffer at 4°C in a 30-kDa concentrator tube at least three times and the labeled proteins were collected. ParB-Cy5 and ParB-AF555 protein were further concentrated and stored at –80°C before use.

Fluorescence-combined optical tweezers assays

A dual-optical tweezer setup combined with confocal microscopy and microfluidics (LUMICKS, C-trap) was used to perform the single-molecule assays (38,39). In brief, a 1064-nm fiber laser and a water-immersion objective were used to create two orthogonally polarized optical traps. The trap separation was controlled using a piezo mirror for beam-steering one trap. Force measurements were performed by back-focal plane interferometry of the condenser top lens using a position-sensitive detector. A computer-controlled stage enabled rapid movement of the optical traps within a multiple-channel flow cell (36). This microfluidic system allowed for the rapid in situ construction and characterization of DNA dumbbell constructs, and facilitated the swift transfer of tethered DNA between different flow channels (Figure 1A). DNA molecules were captured between two streptavidin-coated polystyrene beads (4.38 or 1.76 μm in diameter) using the multichannel laminar flow cell and were tensioned by increasing the distance between the optical traps. The presence of a single suspended DNA molecule was verified by its inherent mechanical force-extension relationship (40). The DNA tether was then transported to the protein or buffer channel as described for each assay. In these channels, a constant force was applied to the DNA tether via a high-frequency feedback system on the steered trap during data acquisition. Unless stated otherwise, all experiments were carried out in reaction buffer containing 20 mM Tris–HCl pH 7.5, 50 mM NaCl and 2 mM $MgCl_2$ with a constant force of 1 pN exerted on the DNA template.

Confocal scans were performed when DNA tethers were in the buffer and protein channels. A 488-nm laser was used for imaging ParB-eGFP, a 532-nm laser was used for imaging ParB-AF555, and a 638-nm laser was used for imaging ParB-Cy5 and To-Pro-3. Kymographs were generated via a confocal line scan through the center of the two beads with a pixel size of 75 nm for 0.1 ms.

Single-molecule data analysis

Single-molecule fluorescence data of ParB binding to the dsDNA obtained from the single-molecule experiment were analyzed using custom software provided by LUMICKS. DNA force and extension data were taken at 100 Hz. DNA-bound ParB molecules were quantified by the measurement of the fluorescence intensity. The overall fluorescence intensity along the DNA (the total number of photons in each column of the kymograph) as a function of time was fitted by an exponential function. The fluorescence intensity of a ParB multimer was calculated as the number of photons in the manually selected region.

The diffusion of ParB multimers along the dsDNA was quantified by tracking the position of the multimer in each frame. Briefly, kymograph segments containing diffusive ParB multimers were generated with reduced background noise using Fiji (41). The position of a multimer in each frame was determined as the largest fluorescence intensity using MATLAB. The movement of a ParB multimer in nm was converted to base pairs using the force–extension characteristics of DNA (42). The sliding processivity was defined as the average distance that the ParB multimer slides before reversing the direction of motion or stalling. Due to the limited spatial resolution, only sliding distances over 1 kb were counted in statistics. The sliding rate of the ParB multimer was obtained from a linear fit to the trajectory of each sliding event. The diffusion coefficients were measured as a linear fit to the one-dimensional mean square displacement (MSD) taken within 50 s at a 5-s interval (43).

RESULTS

ParB proteins stochastically multimerize on and stably bind to nonspecific DNA

We first sought to explore the dynamic association of ParB with nonspecific DNA containing no *parS* sites (hereafter referred to as nsDNA) at the single-molecule level. To this aim, we employed a fluorescence-combined dual-trap optical tweezers setup to monitor protein-DNA interactions in real time (44). This single-molecule experiment was performed in a four-channel microfluidic system, which allows for the quick formation of a single DNA tether (in channels 1 and 2) and the rapid switching of experimental conditions (in channels 3 and 4) (Figure 1A) (44). Figure 1A displays

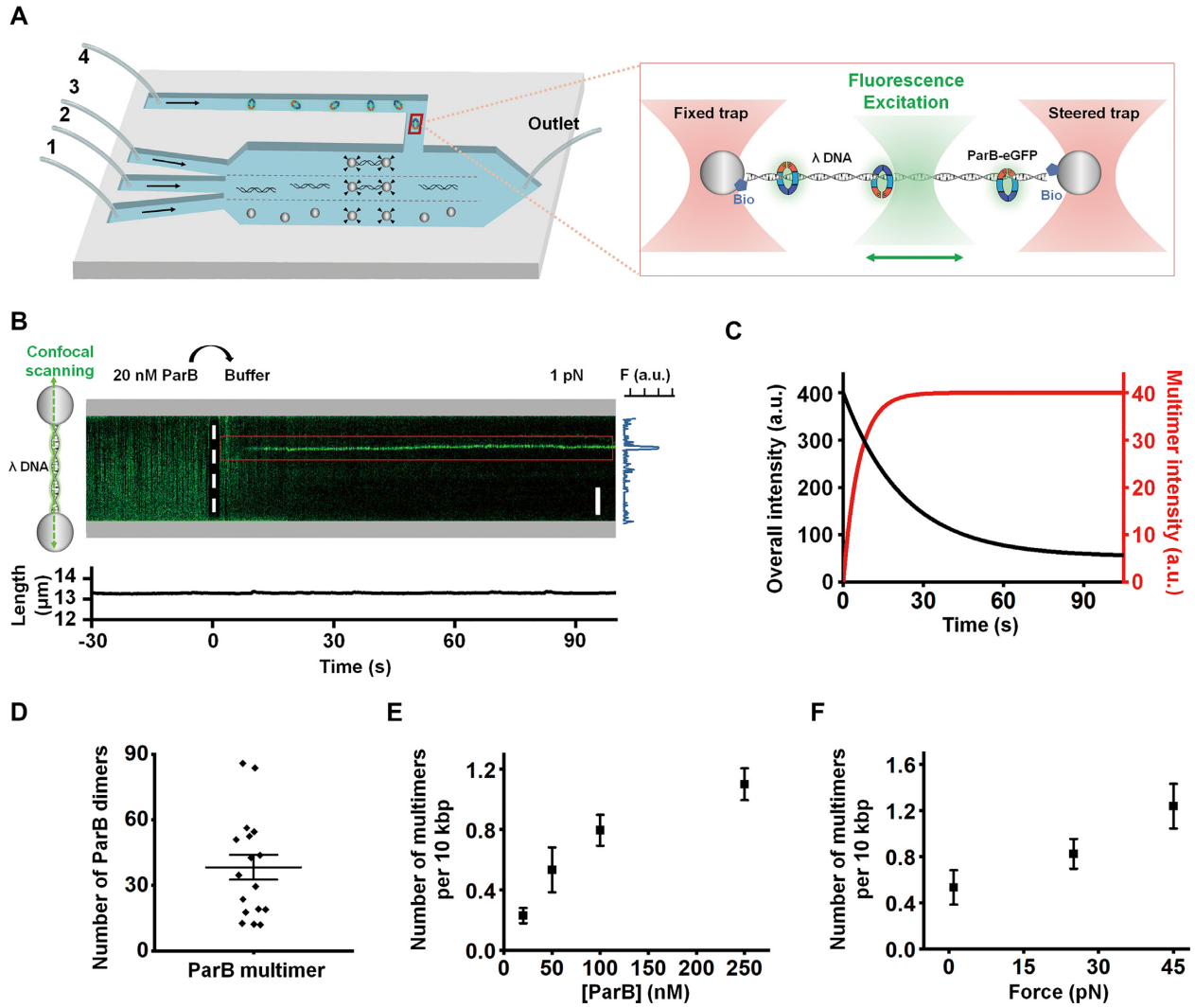

Figure 1. Stochastic multimerization and stable binding of ParB proteins on DNA. (**A**) Schematic of the experimental setup and configuration. A single DNA tether was formed in channels 1–3 containing streptavidin-coated beads, biotinylated λ DNA, and reaction buffer, respectively. The successfully formed DNA tether was moved to protein channel 4 for ParB loading and imaging, followed by transporting back to buffer channel 3 for imaging. On the right, a zoomed-in view illustrates the experimental configuration (not to scale). (**B**) A representative kymograph and DNA length versus time of a suspended λ DNA showing ParB binding to the DNA in the protein and subsequent buffer channels. The gray rectangles indicate the beads' positions. The scale bar represents 3 μm. The final fluorescent profile of ParB along the DNA is shown alongside the kymograph. (**C**) Time-evolutions of the overall fluorescence intensity along the DNA (black line) and the fluorescence intensity of the ParB multimer in the buffer channel (red line). (**D**) The number of ParB molecules in multimer formed on nsDNA in the absence of CTP. (**E**) The average number of ParB multimers formed along the λ DNA in the buffer channel after a 1-min incubation in the protein channel containing 20, 50, 100, or 250 nM ParB. $n = 9$, 12, 14 and 15, respectively. The data are shown in mean ± SEM. (**F**) The average number of ParB multimers formed along the λ DNA under a force of 1, 25 and 45 pN in the buffer channel after a 1-min incubation in the 20 nM ParB channel. $n = 12$, 8 and 9, respectively. The data are shown in mean ± SEM.

a schematic of the experimental configuration in which a 48.5-kb λ DNA molecule was suspended between two optical traps via two streptavidin-coated microspheres, while a confocal laser repeatedly scanned along the tensioned DNA to detect the dynamic interplay between fluorescently labeled proteins and the DNA.

In this experiment, following the confirmation of a single DNA molecule suspended between two microspheres by the inherent force-extension relationship of dsDNA in the buffer channel (no CTP) (42), we transported the tether to the protein channel containing 20 nM ParB-eGFP and incubated for 1 min while maintaining a constant force of 1 pN on the tether. In this channel, the kymograph of the DNA molecule indicates a uniform coating by ParB possibly in a dimeric form, while the DNA length remained unchanged (Figure 1B). DNA condensation induced by ParB coating was reported by previous studies (20,37). Given the recapitulation of DNA condensation under 250 nM ParB and 0.1 pN force (Supplementary Figure S3), this discrepancy can be reconciled by the low ParB concentration and the relatively high force used in our assay.

To gain insight into the DNA dissociation properties of ParB, we switched the ParB-coated DNA tether back to the buffer channel, wherein a majority of ParB proteins were found to dissociate from the DNA within tens of seconds, as reflected by a gradual decay of the overall fluorescence

intensity of the DNA molecule over time (Figure 1B, C and Supplementary Figure S4A). Intriguingly, other than dissociation, we were also surprised to detect the appearance of fluorescence spots that were gradually and stochastically formed along the DNA (Figure 1B). Analysis of the intensity of these fluorescence spots as a function of time indicated that it typically took tens of seconds for them to reach equilibrium (Figure 1C). Given the absence of free ParB proteins in the buffer channel, these fluorescence spots are attributable to the spontaneous multimerization of DNA-bound ParB proteins. The gradual dissociation of nonmultimeric ParB proteins likely provides space on DNA that triggers the short-distance movement and cluster of the remaining proteins, resulting in stochastic protein assembly. Notably, these ParB multimers were found to stably bind to DNA and remain nearly static for a long period (over 5 min) (Supplementary Figure S4A). In the ParB channel, we also detected the binding of ParB multimers to the DNA in some cases, and consistently, the DNA binding status was maintained in the buffer channel (Supplementary Figure S5). The characteristic of the ParB multimer to stably bind to DNA is further substantiated by a protein exchange assay (Supplementary Figure S6). Control experiments under a high salt condition (100 mM NaCl) and with ParB labeled with Cy5 (ParB-Cy5) or Alexa Fluor 555 (ParB-AF555) produced similar observations, excluding the possibility that the formation of the ParB multimer was due to the low salt condition (50 mM NaCl) or to the eGFP used for the fluorescence detection (Supplementary Figures S5 and S6).

Next, we characterized the intrinsic properties of the ParB multimer on DNA. Calculating the fluorescence intensities of ParB-eGFP multimers and comparing them with a single DNA-bound dCas9-eGFP/sgRNA complex allows us to determine an average of 76 monomers (38 dimers) in each ParB multimer (Figure 1D and Supplementary Figure S7) (45). Moreover, both increased ParB concentration and applied force on DNA (during incubation) facilitated the formation of ParB multimers (Figure 1E, F). Collectively, our data demonstrate that ParB can spontaneously multimerize on nsDNA in a stochastic, CTP-independent manner. Unlike nonmultimeric ParB proteins that only transiently interact with nsDNA, the ParB multimer retains stable binding to nsDNA.

CTP facilitates the formation and diffusion of the ParB multimer along DNA

Since ParB has proven to be a CTPase (17,18,23), we next asked whether and how CTP regulates multimerized ParB. Through examining the status of DNA-bound ParB, we found that nonmultimeric ParB proteins on the DNA showed an even faster dissociation in the buffer channel containing 2 or 10 mM CTP (Supplementary Figure S4), and yet the number of the ParB multimer increased by approximately threefold (Figure 2A and Supplementary Figure S8). Meanwhile, the DNA length remained unchanged in the CTP channel. Strikingly, in contrast to the nearly static ParB multimers without CTP, the presence of CTP featured an apparent diffusion of 79% of ParB multimers ($n = 261$) along the DNA for a few minutes (Figure 2B and Supplementary Figure S4B). The CTP-driven diffusion of the ParB multimer was also corroborated by experiments with ParB-Cy5 and ParB-AF555 (Supplementary Figure S9). To quantitatively characterize the diffusion, we derived corresponding trajectories of individual multimer from the kymographs (see methods), based on which the sliding rate, processivity (defined as the average speed and distance that a ParB multimer maintains a unidirectional movement before stalling or reversing its direction of motion), and diffusion coefficient of ParB multimers were measured (Figure 2B and Supplementary Figure S10A). It turned out that all three parameters increased with increasing CTP concentration (Figure 2C–E and Supplementary Figure S10B), consistent with the notion that CTP promotes diffusion. Although the CTP concentration used here is above the *in vivo* condition (0.8 mM CTP), it is noteworthy that our measured diffusion coefficients of ParB multimers are in good agreement with the *in vivo* measurements by super-resolution microscopy (25,46).

To address whether CTP binding is sufficient to support the diffusion of the ParB multimer, we further assayed two ParB mutants: N112S, which can bind CTP without hydrolysis, and R80A, which is deficient in both CTP binding and hydrolysis (Supplementary Figure S2C) (17). Despite the capability of both mutants to multimerize, the R80A multimer barely diffused and the N112S multimer showed reductions in diffusion coefficient and processivity but a comparable diffusion rate with ParB (Supplementary Figure S11). Therefore, it is likely that both CTP binding and hydrolysis are required for the efficient diffusion of the ParB multimer.

The ParB multimer preferentially remains immobile on *parS* sites and can absorb a diffusive one

We next addressed how *parS* motifs modulate the ParB multimer. To this end, we first constructed a 21.5-kb DNA template containing an 8× *parS* sequence located 7.8-kb to one end and 13.3-kb to the other (Figure 3A and Supplementary Figure S1A). After incubation in the ParB channel for 1 min, up to 75% of examined DNA molecules (n = 24) showed a ParB multimer binding around the 8× *parS* region with the DNA length maintained (Figure 3A). Alternating the position and depletion of the 8x *parS* sequences along the DNA substantiated that the observed DNA binding by the ParB multimer is indeed a result of the presence of the *parS* sites (Supplementary Figure S12). Surprisingly, compared to the multimers on nsDNA, 8× *parS*-bound multimers were distinguished in their response to the presence of CTP and preferentially remained immobile on the sites for minutes (Figure 3A). The presence of 10 mM CTP supports only 2 out of 23 *parS*-bound ParB multimers diffusing away in 10 min (Supplementary Figure S13A).

We next asked whether the inertia of *parS*-bound ParB multimers in the presence of CTP is because of the excess *parS* sites designed in our DNA template. We thus reduced the copy number of *parS* motifs and examined the association of ParB multimers with a 1× *parS*-containing DNA template. After the ParB channel incubation, only 2 out of 14 examined DNA molecules showed a ParB multimer binding at the 1× *parS* motif (Figure 3B). However, in the buffer channel, diffusive ParB multimers were found to

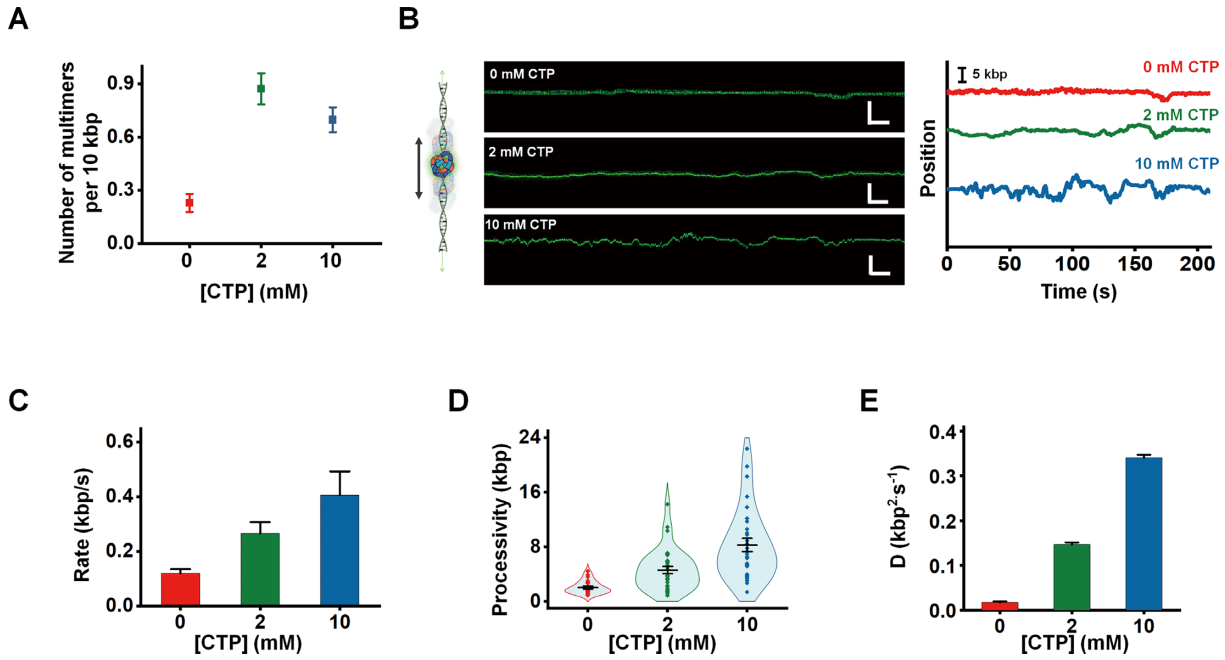

Figure 2. The diffusion of ParB multimers along DNA in the presence of CTP. (**A**) The average number of ParB multimers on DNA in the presence of 0, 2 or 10 mM CTP after a 1-min incubation in the 20 nM ParB channel. The error bars represent SEM. $n = 11$, 23 and 26, respectively. (**B**) Representative kymographs and derived real-time trajectories of individual ParB multimers showing their movements in the presence of 0, 2 or 10 mM CTP. Scale bars represent 5 μm and 10 s, respectively. (**C**) The sliding rate of ParB multimers in the presence of 0, 2 or 10 mM CTP. The data are shown in mean ± SEM. (**D**) The sliding processivity of ParB multimers in the presence of 0, 2 or 10 mM CTP. (**E**) The diffusion coefficient of ParB multimers in the presence of 0, 2 or 10 mM CTP. $n = 23$, 32 and 30, respectively.

switch to be immobile on the site ($n = 7$) (Figure 3B). Consistently, only 3 out of 12 1× *parS*-bound ParB multimers were capable of escaping from the site and diffusing away in 10 min (Supplementary Figure S13B). These data suggest that the ParB multimer can recognize *parS* motifs and prefer to stay immobile on them, and the immobility of the ParB multimer on *parS* is only moderately regulated by the number of the *parS* motif.

Since ParB multimers preferentially stay stationary on *parS* sites, other diffusive ones would inevitably bump into immobile *parS*-binding multimers (Figure 3C). We thus examined the consequence of a collision of a diffusive ParB multimer with an immobile multimer on *parS* sites. Analysis of the fluorescence intensity revealed that 43% of diffusive ParB multimers ($n = 30$) fused with the immobile *parS*-bound multimers after the collision, and the rest were more inclined to separate and diffuse away from the immobile ones (Figure 3D, E). In both scenarios, the stationary status of *parS*-bound ParB multimers was maintained. Similar collision outcomes occurring on nsDNA were observed (Supplementary Figure S14).

Taken together, the ParB multimer can recognize *parS* motifs and prefers to stably bind to them. Moreover, the *parS*-bound multimer has a chance to absorb diffusive ones after a collision.

The ParB multimer efficiently bridges DNA molecules

Our experiments demonstrated that ParB multimers are composed of tens of ParB dimers and they stably associate with DNA. These findings raised the possibility that the ParB multimer might serve as a hub for the assembly of higher-order DNA structures. To examine that, we performed a DNA catching experiment, wherein we first assembled ParB-eGFP multimers on a suspended λ DNA molecule in a ParB channel and then disassociated nonmultimeric ParB molecules from the DNA in a buffer channel. Following that, we transported the ParB multimer-associated DNA to a channel containing free λ DNA and To-Pro-3 (a DNA dye), wherein fluorescent DNA and ParB were simultaneously monitored (Figure 4A). As evident by the flow-stretched DNA molecule, 16 out of 29 ParB multimers were detected to connect free λ DNA molecules after a 30-s incubation in the channel (Figure 4B). Note that a ParB multimer capturing multiple DNA molecules was also detected in rare cases (Supplementary Figure S15A). The capability of the ParB multimer to bridge DNA was also demonstrated by the experiments with ParB-Cy5 and is in stark contrast to that of the nonmultimeric ParB which failed to do so (Supplementary Figures S16).

Next, we asked whether the *parS* motif plays a role in the regulation of the DNA bridging capability of the ParB multimer. To answer that, we prepared an 18.6-kbp DNA molecule containing two 8× *parS* motifs separated by 4.4-kb DNA (see methods). We repeated the DNA catching experiment with the replacement of the free λ DNA with this particularly designed *parS*-containing DNA. To our surprise, up to 93% of the ParB multimers ($n = 95$) were monitored to bridge free *parS*-containing DNA (Figure 4C–E). In comparison, experiments with an 18.6-kb DNA containing no *parS* motifs gave rise to the reduction in the percentage of bridging ParB multimers to 50% ($n = 111$) (Figure

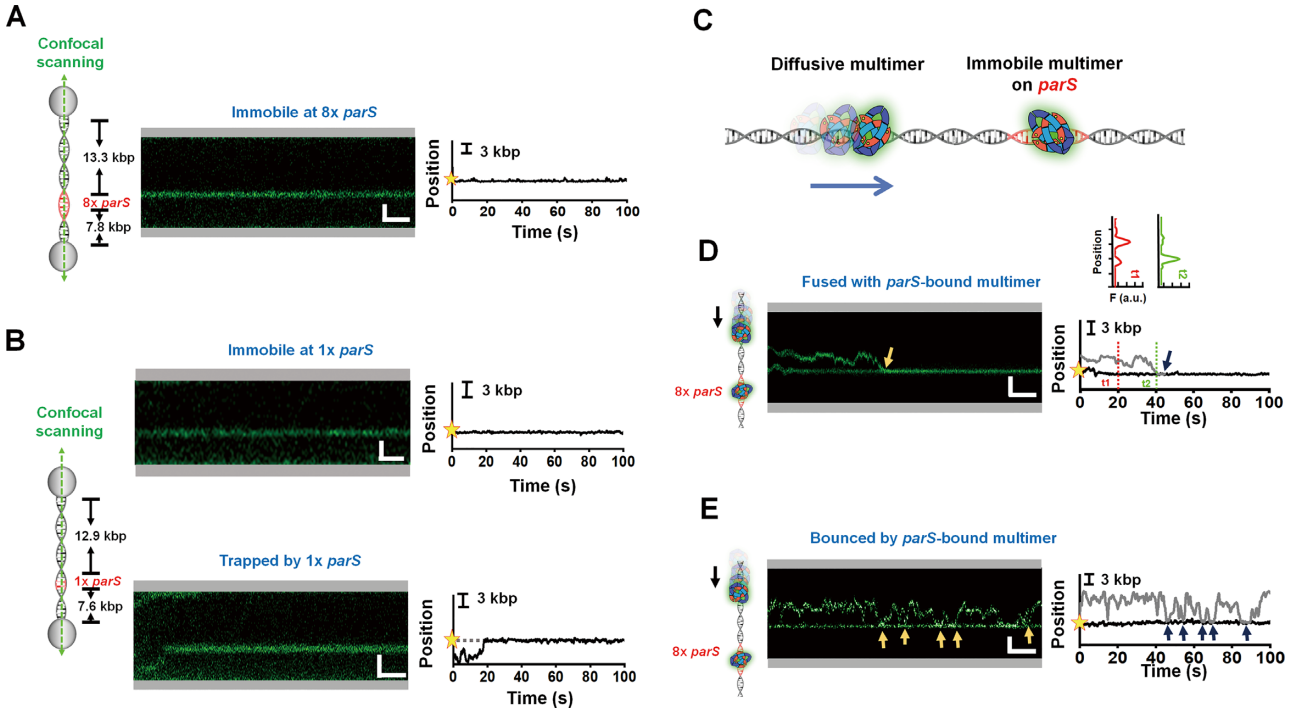

Figure 3. The influence of *parS* sites on diffusive ParB multimers and their collision. (**A**) Schematic of the 8x *parS* DNA template showing the position of the *parS* sites (highlighted in red) in the DNA (not to scale). Representative kymograph and derived real-time trajectory of the ParB multimer showing its binding to the 8× *parS* sites in the presence of 10 mM CTP. The star highlights the position of the 8× *parS* sites. Scale bars represent 2 μm and 10 s, respectively. (**B**) Schematic of the 1× *parS* DNA template showing the position of the *parS* site (highlighted in red) in the DNA (not to scale). Representative kymographs and derived real-time trajectories of ParB multimers showing their binding to or entrapment by the 1× *parS* site. The star indicates the position of the 1× *parS* site. Scale bars represent 2 μm and 10 s, respectively. (**C**) The cartoon of a collision between a diffusive multimer and an immobile one at 8× *parS* sites. (D, E). Representative kymographs and derived real-time trajectories of ParB multimers show that a diffusive multimer either fuses with (**D**) the *parS*-bound multimer or is bounced away (**E**) after a collision. Scale bars represent 2 μm and 10 s, respectively. The yellow and blue arrows highlight the occurrence of collision events. The gray rectangles indicate the beads' positions. The fluorescence intensity profiles at two time points (before and after the collision) are shown above the kymograph.

4D, E). Moreover, depletion of CTP was found to attenuate the bridging capability of the ParB multimer (Supplementary Figure S17).

In summary, the ParB multimer possesses a distinct capability of bridging DNA molecules, which is enhanced with the involvement of CTP and the *parS* sequence in the DNA.

The ParB multimer mediates the transportation of bridged DNA molecules

Having demonstrated that the ParB multimer is capable of diffusing along and bridging DNA molecules, we further asked whether they could mediate the relative motion between bridged DNA molecules. As expected, the movements of ParB multimers complexed with 18.6 kb DNA along λ DNA were monitored in the presence of CTP (Supplementary Figure S18). To avoid the influence of the thermal fluctuation from the long DNA and to increase the spatial resolution, we chose to use a Cy5-labeled 52-bp dsDNA oligonucleotide containing a 1x *parS* motif (*parS*-oligo-Cy5) to accurately record the motion of the ParB multimer-bridged DNA molecules. In this experiment, we incubated a suspended λ DNA in a channel containing the *parS*-oligo-Cy5 and ParB-eGFP for 1 min and then transferred the tether to a buffer channel and waited for the disassembly of the nonmultimeric ParB for 5 minutes before the fluorescence detection (Figure 5A). Through simultaneously scanning the fluorescence signals of ParB and the oligonucleotide, we found that up to 75% of ParB multimers assembled on the λ DNA ($n = 77$) colocalized with the oligonucleotides (Supplementary Figure S19). This finding suggests that the ParB multimer also mediates the bridging of the λ DNA with the oligonucleotide. Consistently, simultaneous movements of the ParB multimer and the oligonucleotide along the λ DNA were recorded (Figure 5B). To quantitatively characterize the movements, we derived corresponding trajectories of the multimer and the *parS*-oligo-Cy5 from the kymographs and found that the diffusion coefficient of the multimer was significantly reduced by the complex with the bridged oligo (Figure 2E and Supplementary Figure S17D).

Given that both the *parS* motif and CTP play a regulatory role in DNA bridging, we speculated that both of them also modulate the DNA transporting capability of the ParB multimer. To test that, we first revisited the experiments with a 58-bp oligonucleotide containing nonspecific sequences (ns-oligo-Cy5) for comparison. We found that the number of the ParB multimer-oligonucleotide complex formed on the λ DNA was reduced by approximately threefold (Figure 5C). Moreover, the diffusion of the complex along DNA was often interrupted by a sudden release of the nonspecific oligonucleotide (Figure 5D). The statisti-

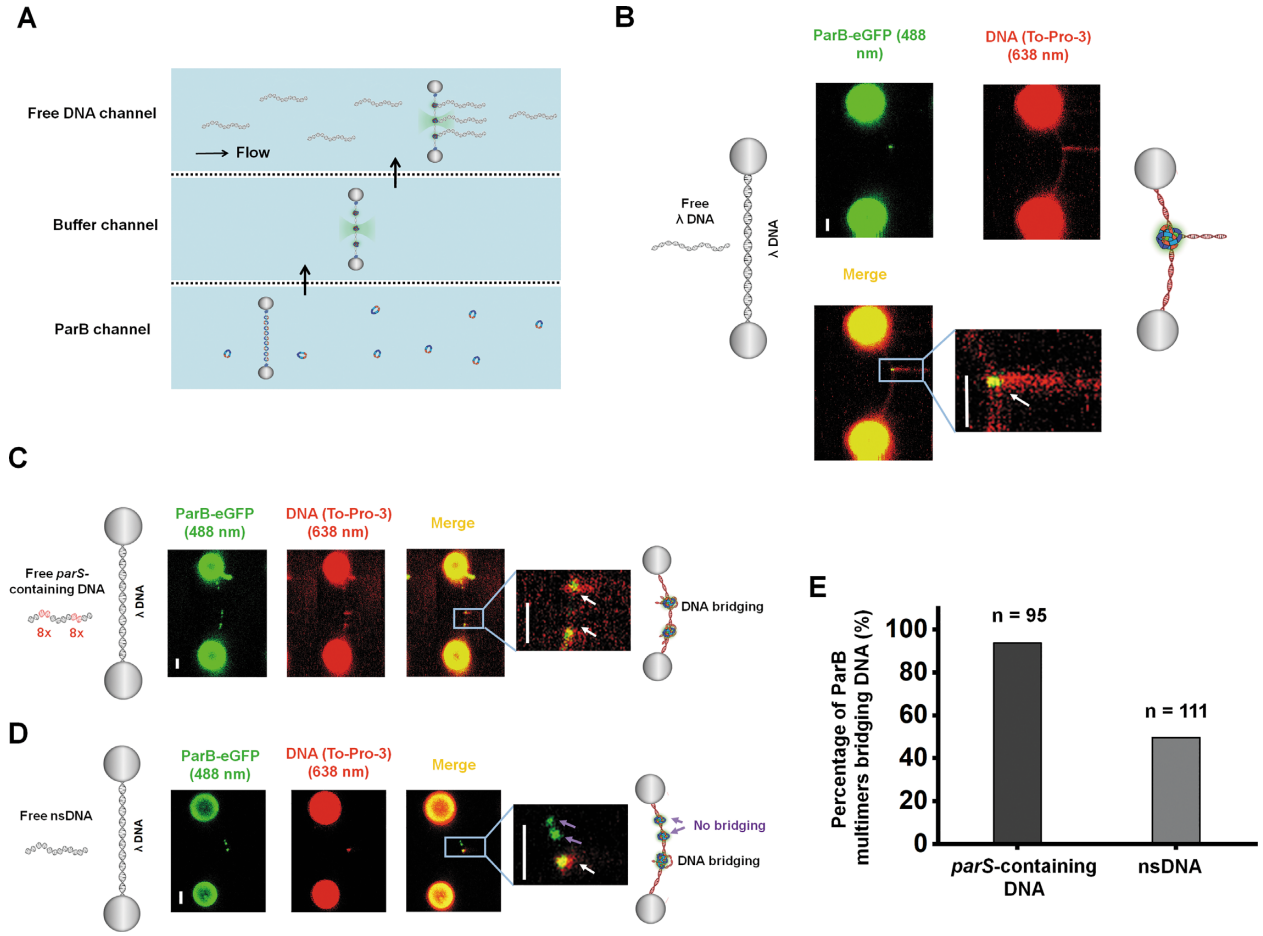

Figure 4. The ParB multimer bridges two DNA molecules. (**A**) Schematic representation of the procedures of the DNA catching assay. A suspended λ DNA under 1 pN is sequentially incubated in the ParB channel for protein loading, the buffer channel for nonmultimeric ParB dissociation, and the free DNA channel for DNA catching. Confocal images are taken in the free DNA channel once the flow perpendicular to the suspended DNA is on. (**B**) Representative confocal images and a zoom-in view showings that a suspended λ DNA and a flow-stretched λ DNA (red) are bridged by a ParB multimer (green). (**C**) Representative confocal images and a zoom-in view showing that a suspended λ DNA and flow-stretched *parS*-containing DNA molecules (red) are bridged by ParB multimers (green). (**D**) Representative confocal images and a zoom-in view showing that a ParB multimer (green) bridges a suspended λ DNA and flow-stretched nonspecific DNA molecules (red) and that the other two are not. Scale bar, 2.5 μm. (**E**) The percentage of ParB multimers assembled on λ DNA bridging *parS*-containing or nonspecific DNA.

cal analysis showed that the presence of *parS* prolongs the DNA binding lifetime of the ParB-oligonucleotide complex by approximately 2 times (Figure 5E). The reason for these observations might be ascribed to the attenuation of the ParB multimer-oligonucleotide stability by the absence of *parS*. Consistently, depletion of CTP also attenuates DNA transportation activity of the ParB multimer (Supplementary Figure S17).

Together, we conclude that the ParB multimer is capable of mediating the relative motion between bridged DNA molecules, and this capability is promoted by CTP and the *parS* motif in the bridging DNA region.

DISCUSSION

During bacterial chromosome segregation, proper distribution and assembly of DNA-bound ParB molecules is key to the formation of the partition complex. In this process, ParB dimerization and multimerization confer specificities and functional advantages for DNA spreading and organization. It has been believed that the ParB dimer is the functional unit for spreading (17,18,25,29,47). Nevertheless, our knowledge of how ParB dimers further cluster into a tight focus for the assembly of a higher-order nucleoprotein complex is still limited. In this work, through the real-time visualization of the dynamic association of ParB with nonspecific or *parS*-containing DNA, we discovered that ParB can spontaneously multimerize into higher-order species composed of an average of 38 ParB dimers (Supplementary Figure S7). Notably, the importance of the ParB multimerization is reflected by the finding that the single amino acid mutation in ParB causing a defect in multimerization but not in dimerization also results in a chromosome segregation defect (48). ParB multimerization can take place along nsDNA (Figure 1B). This is possibly realized by the cluster of DNA-bound ParB dimers over a short distance. This pathway restricts the ParB multimer to assemble around *parS* motifs where the ParB dimer maintains a high concentration. Moreover, compared to the ParB dimer, the ParB multimer displayed exceedingly stable binding to nsDNA

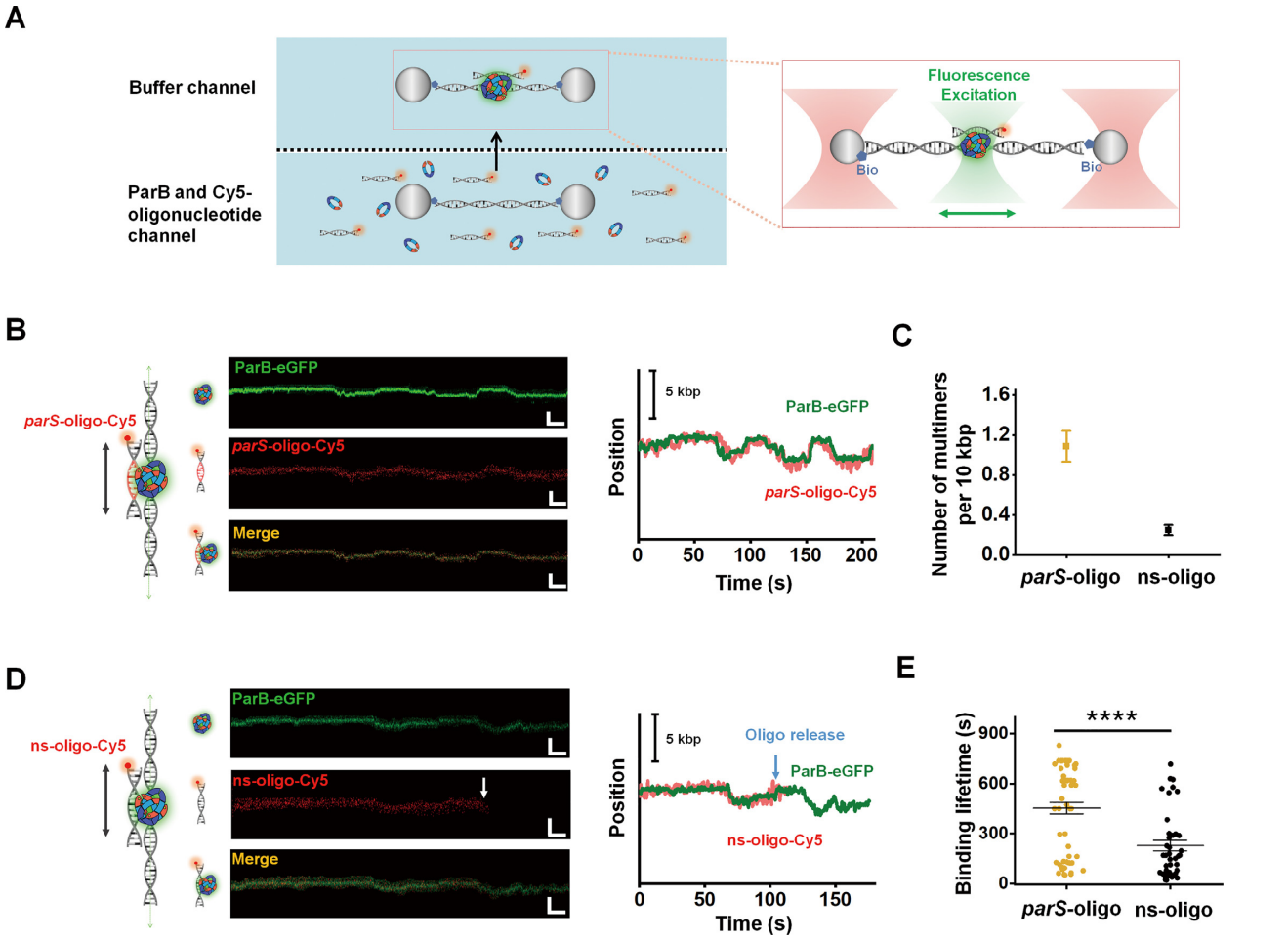

Figure 5. The ParB multimer mediates the relative motion between bridged DNA. (**A**) Schematic of the experimental procedures. A suspended λ DNA tether is incubated in the channel containing 50 nM ParB-eGFP and 2.5 nM Cy5-labeled oligonucleotide, followed by transportation of the tether to the buffer channel wherein fluorescent signals of the protein and the oligonucleotide are recorded (right). (**B**) Representative kymographs and derived real-time trajectories of a ParB multimer (green) and *parS*-oligo-Cy5 (red) showing their movements in the presence of 2 mM CTP. Scale bars represent 3 μm and 10 s, respectively. (**C**) The average number of multimer-oligo complexes assembled on λ DNA in the presence of 2 mM CTP. *parS* and ns represent *parS*-containing and nonspecific oligonucleotide, respectively. The data are shown in mean ± SEM. $n = 11$ and 34, respectively. (**D**) Representative kymographs and derived real-time trajectories of a ParB multimer and ns-oligo-Cy5 showing their movements in the presence of 2 mM CTP. The arrow highlights a sudden release of the oligonucleotide from the ParB multimer. Scale bars represent 1.5 μm and 10 s, respectively. (**E**) The DNA-associating lifetime of the complex formed by *parS*-containing or nonspecific oligonucleotide and the ParB multimer. The data are shown in mean ± SEM. $n = 58$ and 42, respectively. $^{****}P < 0.0001$

even in the presence of CTP (Supplementary Figure S4). Considering that there are a large number of DNA-binding proteins acting as roadblocks *in vivo*, ParB may also benefit from the stochastic multimerization in avoiding barriers and accessing distant DNA. In *B. subtilis*, DNA segregation proceeds coordinately with replication (14,33). There is a chance that the stable binding of the ParB multimer impedes other DNA transactions, such as replication. However, ParB multimers are quite mobile, especially the ones on nsDNA. After a collision with DNA-based motor proteins, the ParB multimer may switch the direction of movements and even dissociate. The coordination of the ParB-DNA assembly with other DNA transactions and the potential role of the ParB multimer in recruiting the SMC complex warrant further exploration (12,49).

DNA-based diffusion is deemed as one of the effective means for ParB to spread along and assemble DNA. In addition, ParB diffusion has also been speculated to function in the effective transportation and modulation of chromosomal DNA, though direct evidence is lacking (50). A laminar flow-based single-molecule study provided the first direct evidence of the diffusion of the ParB dimer, in which quantification of ParB movement without the presence of any nucleotides revealed a diffusion coefficient of 3.0 kb^2/s or 0.34 $\mu m^2/s$ (29). Recently, direct visualization of CTP-driven diffusion of quantum dot-labeled ParB was conducted by Balaguer *et al.* (20). Although they did not determine the multimeric state of diffusive ParB, the reported diffusion coefficient (3.5 kb^2/s or 0.41 $\mu m^2/s$) agrees with the previous one but is an order of magnitude higher than we measured here for ParB multimers (0.1–0.4 kb^2/s or 0.01–0.05 $\mu m^2/s$) (Figure 2E). Moreover, the fast diffusion detected in their work differs from our observations in that it often lasts a few seconds and culminates in a quick

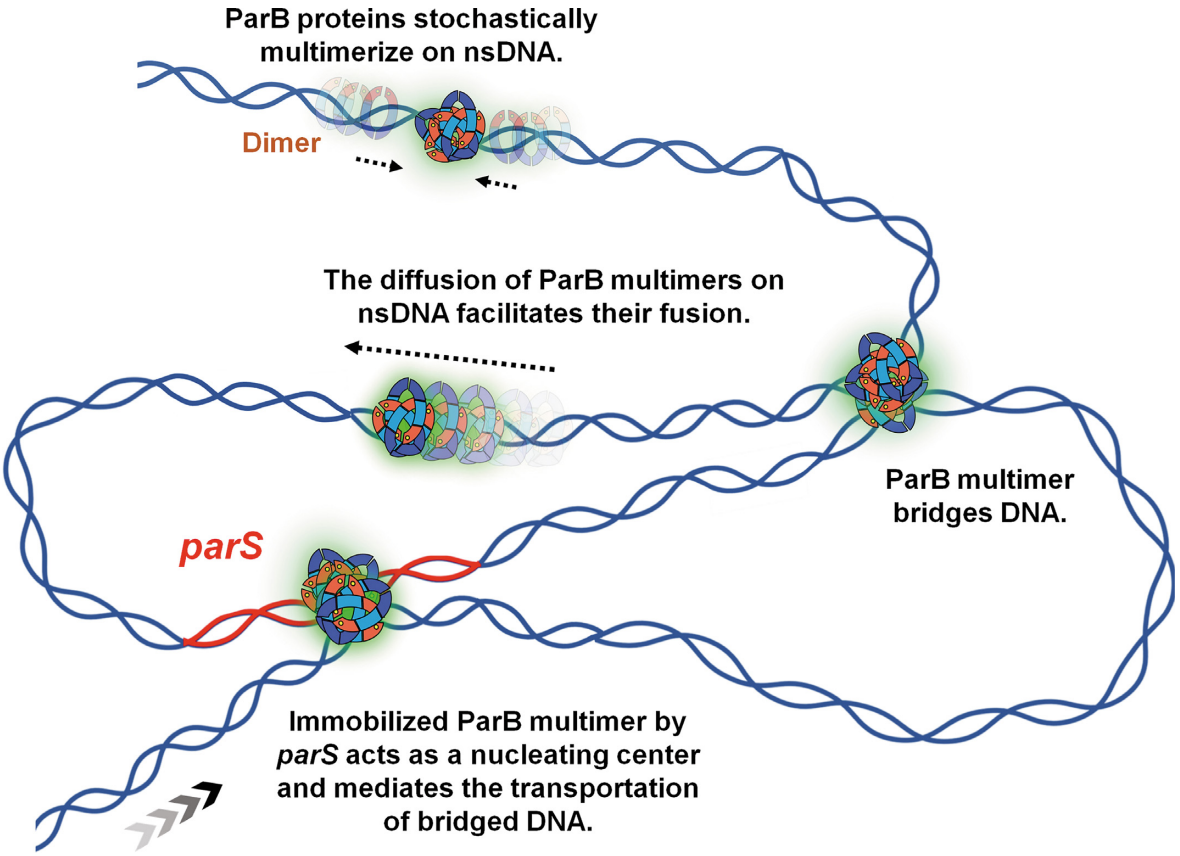

Figure 6. A model of the ParB multimer functioning in partition complex assembly. The ParB dimer forms a ring-shaped structure that encircles dsDNA. The movement of ParB dimers (short arrows) allows for the stochastic formation of ParB multimers (shown as a group of ParB dimers) along nsDNA. The diffusion of ParB multimers (long arrow) along nsDNA helps to reach and compact distance DNA and to further aggregate. ParB multimers bound to *parS* sites (red) remain immobile and act as a nucleating center to bring in DNA via active DNA transportation (progressive arrows).

DNA dissociation of ParB molecules. It is reasonable that ParB multimers diffuse along DNA more slowly than ParB dimers as DNA binding motifs accumulate within ParB multimers. Moreover, other than DNA spreading realized by the ParB dimer, the relatively slow diffusion of the ParB multimer may serve a different purpose in organizing chromosomal DNA into higher-order structures, such as DNA transportation and ParB condensation (see discussion below). This speculation is reinforced by the finding that 95% of ParB molecules within ParB condensates display slow mobility *in vivo*, with a similar coefficient of 0.43 kb^2/s or 0.05 $\mu m^2/s$ (25). It is plausible that the specific functions of ParB in different partitioning steps are regulated by the multimeric status of the protein.

Since the discovery of the CTPase activity of ParB, tremendous efforts have been devoted to the investigation of the regulatory roles of CTP in ParB binding to *parS* and spreading. CTP binding has proven to sufficiently support the sliding of the ParB dimer, whereas CTP hydrolysis serves as a timing control to limit the sliding and recycle the proteins (21). Our work provides additional functional roles of CTP in regulating ParB activity. First, compared to the enhanced dissociation of the nonmultimeric ParB (Supplementary Figure S4), CTP has an opposite effect on ParB multimers and promotes their assembly on nsDNA (Figure 2A). Second, CTP also promotes the diffusion of the ParB multimer (Figure 2). Third, CTP contributes to DNA bridging and transportation mediated by the ParB multimer (Figure 5 and Supplementary Figure S17). These findings broaden the functionalities of CTP in the regulation of ParB activity.

The ParB multimer is distinguished from the ParB dimer in its unique capabilities to bridge and transport two DNA molecules (Figures 4 and 5). Moreover, the preference of the ParB multimer in stably binding to *parS* sites also differs from that of the ParB dimer (20). These characteristics possibly originate from multiple DNA binding motifs in the multimers and may prepare them as essential docking points for the organization of the network of DNA loops in partition complex assembly. Additionally, diffusive ParB multimers have a chance to fuse and grow after a collision on both *parS* and nonspecific DNA (Figure 3 and Supplementary Figure S14); this random collision could serve as a means for ParB to further assemble into foci. Based on our findings, we proposed a model of the ParB multimer functioning in the assembly of the partition complex. As illustrated in Figure 6, spontaneous multimerization of ParB dimers stochastically occurs on nsDNA; Non-*parS*-bound multimers diffuse along DNA to access distance DNA; The *ParS*-bound ParB multimer stays stationary and serves as a nucleation center; The distinguished capability of the ParB multimer to simultaneously bind to

and actively transport DNA molecules allow for the formation and modulation of DNA loops; The collision and fusion of diffusive ParB multimer along DNA facilitate ParB–DNA nucleation. Our model at least partially explains how dispersed ParB dimers, after spreading, cluster and organize the *parS*-flanking DNA. It also shares similarities with the previously proposed nucleation and caging model (26), such as the immobility of ParB bound to *parS* and ParB–nsDNA interaction, and ParB multimerization along with DNA bridging and transportation may help prime the nucleation. Overall, this work provides new insights into ParB self-multimerization as well as the potential roles of the ParB multimer in the partition complex assembly during bacterial chromosome segregation.

DATA AVAILABILITY

All data are available from the corresponding authors upon reasonable request and/or included in the manuscript as figure source data or supplementary data.

SUPPLEMENTARY DATA

Supplementary Data are available at NAR Online.

ACKNOWLEDGEMENTS

We thank all the staff of the molecular and cell biology core facility of the School of Life Science and Technology at ShanghaiTech University for providing technical support.
Author contributions: B.S. conceived the project and supervised all research. L.G. and Y.Z. conducted all experiments. L.G., Y.Z., C.L., H.M. and B.S. analyzed and interpreted the data. Q.Z., F.Y. and H.M. helped with the protein purification. L.B., X.Z. and T.W. participated in the DNA template preparation. B.S., L.G. and Y.Z. wrote the manuscript with inputs from all authors.

FUNDING

National Natural Science Foundation of China [32022048, 32100993]; Natural Science Foundation of Shanghai [19ZR1434100, 22ZR1441900]. Funding for open access charge: National Natural Science Foundation of China [32022048].
Conflict of interest statement. None declared.

REFERENCES

1. Badrinarayanan,A., Le,T.B. and Laub,M.T. (2015) Bacterial chromosome organization and segregation. *Annu. Rev. Cell Dev. Biol.*, **31**, 171–199.
2. Santaguida,S. and Amon,A. (2015) Short- and long-term effects of chromosome mis-segregation and aneuploidy. *Nat. Rev. Mol. Cell Biol.*, **16**, 473–485.
3. Sherratt,D.J., Lau,I.F. and Barre,F.X. (2001) Chromosome segregation. *Curr. Opin. Microbiol.*, **4**, 653–659.
4. Wang,X., Montero Llopis,P. and Rudner,D.Z. (2013) Organization and segregation of bacterial chromosomes. *Nat. Rev. Genet.*, **14**, 191–203.
5. Jalal,A.S.B. and Le,T.B.K. (2020) Bacterial chromosome segregation by the ParABS system. *Open Biol*, **10**, 200097.
6. Funnell,B.E. (2016) ParB partition proteins: complex formation and spreading at bacterial and plasmid centromeres. *Front. Mol. Biosci.*, **3**, 44.
7. Rodionov,O., Lobocka,M. and Yarmolinsky,M. (1999) Silencing of genes flanking the P1 plasmid centromere. *Science*, **283**, 546–549.
8. Lin,D.C. and Grossman,A.D. (1998) Identification and characterization of a bacterial chromosome partitioning site. *Cell*, **92**, 675–685.
9. Hwang,L.C., Vecchiarelli,A.G., Han,Y.W., Mizuuchi,M., Harada,Y., Funnell,B.E. and Mizuuchi,K. (2013) ParA-mediated plasmid partition driven by protein pattern self-organization. *EMBO J.*, **32**, 1238–1249.
10. Easter,J. Jr and Gober,J.W. (2002) ParB-stimulated nucleotide exchange regulates a switch in functionally distinct ParA activities. *Mol. Cell*, **10**, 427–434.
11. Ebersbach,G. and Gerdes,K. (2004) Bacterial mitosis: partitioning protein ParA oscillates in spiral-shaped structures and positions plasmids at mid-cell. *Mol. Microbiol.*, **52**, 385–398.
12. Sullivan,N.L., Marquis,K.A. and Rudner,D.Z. (2009) Recruitment of SMC by ParB-parS organizes the origin region and promotes efficient chromosome segregation. *Cell*, **137**, 697–707.
13. Wilhelm,L., Burmann,F., Minnen,A., Shin,H.C., Toseland,C.P., Oh,B.H. and Gruber,S. (2015) SMC condensin entraps chromosomal DNA by an ATP hydrolysis dependent loading mechanism in bacillus subtilis. *Elife*, **4**, e06659.
14. Lee,P.S., Lin,D.C., Moriya,S. and Grossman,A.D. (2003) Effects of the chromosome partitioning protein Spo0J (ParB) on oriC positioning and replication initiation in bacillus subtilis. *J. Bacteriol.*, **185**, 1326–1337.
15. Thanbichler,M. and Shapiro,L. (2006) MipZ, a spatial regulator coordinating chromosome segregation with cell division in caulobacter. *Cell*, **126**, 147–162.
16. Lynch,A.S. and Wang,J.C. (1995) SopB protein-mediated silencing of genes linked to the sopC locus of escherichia coli f plasmid. *Proc. Natl. Acad. Sci. U.S.A.*, **92**, 1896–1900.
17. Soh,Y.M., Davidson,I.F., Zamuner,S., Basquin,J., Bock,F.P., Taschner,M., Veening,J.W., De Los Rios,P., Peters,J.M. and Gruber,S. (2019) Self-organization of parS centromeres by the ParB CTP hydrolase. *Science*, **366**, 1129–1133.
18. Jalal,A.S., Tran,N.T. and Le,T.B. (2020) ParB spreading on DNA requires cytidine triphosphate in vitro. *Elife*, **9**, e53515.
19. Osorio-Valeriano,M., Altegoer,F., Das,C.K., Steinchen,W., Panis,G., Connolley,L., Giacomelli,G., Feddersen,H., Corrales-Guerrero,L., Giammarinaro,P.I. *et al.* (2021) The CTPase activity of ParB determines the size and dynamics of prokaryotic DNA partition complexes. *Mol. Cell*, **81**, 3992–4007.
20. Balaguer,F.A., Aicart-Ramos,C., Fisher,G.L., de Braganca,S., Martin-Cuevas,E.M., Pastrana,C.L., Dillingham,M.S. and Moreno-Herrero,F. (2021) CTP promotes efficient parb-dependent DNA condensation by facilitating one-dimensional diffusion from parS. *Elife*, **10**, e67554.
21. Antar,H., Soh,Y.M., Zamuner,S., Bock,F.P., Anchimiuk,A., De los Rios,P. and Gruber,S. (2021) Relief of ParB autoinhibition by parS DNA catalysis and recycling of ParB by CTP hydrolysis promote bacterial centromere assembly. *Sci. Adv.*, **7**, eabj2854.
22. Jalal,A.S., Tran,N.T., Stevenson,C.E., Chimthanawala,A., Badrinarayanan,A., Lawson,D.M. and Le,T.B. (2021) A CTP-dependent gating mechanism enables ParB spreading on DNA. *Elife*, **10**, e69676.
23. Osorio-Valeriano,M., Altegoer,F., Steinchen,W., Urban,S., Liu,Y., Bange,G. and Thanbichler,M. (2019) ParB-type DNA segregation proteins are CTP-Dependent molecular switches. *Cell*, **179**, 1512–1524
24. Jalal,A.S.B., Tran,N.T., Wu,L.J., Ramakrishnan,K., Rejzek,M., Gobbato,G., Stevenson,C.E.M., Lawson,D.M., Errington,J. and Le,T.B.K. (2021) CTP regulates membrane-binding activity of the nucleoid occlusion protein noc. *Mol. Cell*, **81**, 3623–3636.
25. Guilhas,B., Walter,J.C., Rech,J., David,G., Walliser,N.O., Palmeri,J., Mathieu-Demaziere,C., Parmeggiani,A., Bouet,J.Y., Le Gall,A. *et al.* (2020) ATP-Driven separation of liquid phase condensates in bacteria. *Mol. Cell*, **79**, 293–303.
26. Sanchez,A., Cattoni,D.I., Walter,J.C., Rech,J., Parmeggiani,A., Nollmann,M. and Bouet,J.Y. (2015) Stochastic self-assembly of ParB proteins builds the bacterial DNA segregation apparatus. *Cell Syst.*, **1**, 163–173.

27. Bouet,J.Y., Rech,J., Egloff,S., Biek,D.P. and Lane,D. (2005) Probing plasmid partition with centromere-based incompatibility. *Mol. Microbiol.*, **55**, 511–525.
28. Bingle,L.E., Macartney,D.P., Fantozzi,A., Manzoor,S.E. and Thomas,C.M. (2005) Flexibility in repression and cooperativity by KorB of broad host range incp-1 plasmid RK2. *J. Mol. Biol.*, **349**, 302–316.
29. Graham,T.G., Wang,X., Song,D., Etson,C.M., van Oijen,A.M., Rudner,D.Z. and Loparo,J.J. (2014) ParB spreading requires DNA bridging. *Genes Dev.*, **28**, 1228–1238.
30. Lim,H.C., Surovtsev,I.V., Beltran,B.G., Huang,F., Bewersdorf,J. and Jacobs-Wagner,C. (2014) Evidence for a DNA-relay mechanism in parabs-mediated chromosome segregation. *Elife*, **3**, e02758.
31. Debaugny,R.E., Sanchez,A., Rech,J., Labourdette,D., Dorignac,J., Geniet,F., Palmeri,J., Parmeggiani,A., Boudsocq,F., Anton Leberre,V. *et al.* (2018) A conserved mechanism drives partition complex assembly on bacterial chromosomes and plasmids. *Mol. Syst. Biol.*, **14**, e8516.
32. Errington,J. (2001) Septation and chromosome segregation during sporulation in bacillus subtilis. *Curr. Opin. Microbiol.*, **4**, 660–666.
33. Lee,P.S. and Grossman,A.D. (2006) The chromosome partitioning proteins soj (ParA) and Spo0J (ParB) contribute to accurate chromosome partitioning, separation of replicated sister origins, and regulation of replication initiation in bacillus subtilis. *Mol. Microbiol.*, **60**, 853–869.
34. Breier,A.M. and Grossman,A.D. (2007) Whole-genome analysis of the chromosome partitioning and sporulation protein Spo0J (ParB) reveals spreading and origin-distal sites on the bacillus subtilis chromosome. *Mol. Microbiol.*, **64**, 703–718.
35. Murray,H., Ferreira,H. and Errington,J. (2006) The bacterial chromosome segregation protein Spo0J spreads along DNA from parS nucleation sites. *Mol. Microbiol.*, **61**, 1352–1361.
36. Gross,P., Farge,G., Peterman,E.J. and Wuite,G.J. (2010) Combining optical tweezers, single-molecule fluorescence microscopy, and microfluidics for studies of DNA-protein interactions. *Methods Enzymol.*, **475**, 427–453.
37. Fisher,G.L.M., Pastrana,C.L., Higman,V.A., Koh,A., Taylor,J.A., Butterer,A., Craggs,T., Sobott,F., Murray,H., Crump,M.P. *et al.* (2017) The structural basis for dynamic DNA binding and bridging interactions which condense the bacterial centromere. *Elife*, **6**, e28086.
38. Qin,Z., Bi,L., Hou,X.M., Zhang,S., Zhang,X., Lu,Y., Li,M., Modesti,M., Xi,X.G. and Sun,B. (2020) Human RPA activates BLM's bidirectional DNA unwinding from a nick. *Elife*, **9**, e54098.
39. Bi,L.L., Qin,Z.H., Wang,T., Li,Y.N., Jia,X.S., Zhang,X., Hou,X.M., Modesti,M., Xi,X.G. and Sun,B. (2022) The convergence of head-on DNA unwinding forks induces helicase oligomerization and activity transition. *Proc. Natl. Acad. Sci. U.S.A.*, **119**, e2116462119.
40. Smith,S.B., Cui,Y.J. and Bustamante,C. (1996) Overstretching B-DNA: the elastic response of individual double-stranded and single-stranded DNA molecules. *Science*, **271**, 795–799.
41. Schindelin,J., Arganda-Carreras,I., Frise,E., Kaynig,V., Longair,M., Pietzsch,T., Preibisch,S., Rueden,C., Saalfeld,S., Schmid,B. *et al.* (2012) Fiji: an open-source platform for biological-image analysis. *Nat. Methods*, **9**, 676–682.
42. Marko,J.F. and Siggia,E.D. (1995) Stretching DNA. *Macromolecules*, **28**, 8759–8770.
43. Heller,I., Sitters,G., Broekmans,O.D., Biebricher,A.S., Wuite,G.J. and Peterman,E.J. (2014) Mobility analysis of super-resolved proteins on optically stretched DNA: comparing imaging techniques and parameters. *ChemPhysChem*, **15**, 727–733.
44. Hashemi Shabestari,M., Meijering,A.E.C., Roos,W.H., Wuite,G.J.L. and Peterman,E.J.G. (2017) Recent advances in biological single-molecule applications of optical tweezers and fluorescence microscopy. *Methods Enzymol.*, **582**, 85–119.
45. Schumacher,M.A. and Funnell,B.E. (2005) Structures of ParB bound to DNA reveal mechanism of partition complex formation. *Nature*, **438**, 516–519.
46. Buckstein,M.H., He,J. and Rubin,H. (2008) Characterization of nucleotide pools as a function of physiological state in escherichia coli. *J. Bacteriol.*, **190**, 718–726.
47. Surtees,J.A. and Funnell,B.E. (1999) P1 ParB domain structure includes two independent multimerization domains. *J. Bacteriol.*, **181**, 5898–5908.
48. Kusiak,M., Gapczynska,A., Plochocka,D., Thomas,C.M. and Jagura-Burdzy,G. (2011) Binding and spreading of ParB on DNA determine its biological function in pseudomonas aeruginosa. *J. Bacteriol.*, **193**, 3342–3355.
49. Gruber,S. and Errington,J. (2009) Recruitment of condensin to replication origin regions by ParB/SpoOJ promotes chromosome segregation in b. subtilis. *Cell*, **137**, 685–696.
50. Tisma,M., Panoukidou,M., Antar,H., Soh,Y.M., Barth,R., Pradhan,B., Barth,A., van der Torre,J., Michieletto,D., Gruber,S. *et al.* (2022) ParB proteins can bypass DNA-bound roadblocks via dimer-dimer recruitment. *Sci. Adv.*, **8**, eabn3299.